Interannual variability in the Southern Ocean from an ocean model forced by European Centre for Medium–Range Weather Forecasts reanalysis fluxes

Hans Bonekamp, Andreas Sterl, and Gerbrand J. Komen

Royal Netherlands Meteorological Institute, De Bilt, Netherlands

Abstract. Anomaly patterns in the Southern Ocean in response to variability in the atmospheric forcing are investigated. To this end we forced the Hamburg large-scale geostrophic ocean general circulation model with surface fluxes from the European Centre for Medium–Range Weather Forecasts reanalysis (ERA). ERA covers the period January 1979 through February 1994. First, the atmospheric variability of sea level pressure and the associated wind stress anomalies within the ERA data set are analyzed. An Antarctic Circumpolar Wave type pattern is identified. In the ocean response, sea water temperature and salinity anomalies are found to vary with similar periods. The anomalies advect with the Antarctic Circumpolar Current. High amplitudes occur in the southeast Indian and Pacific Oceans. Sensitivity studies are made, pinning down wind stress and heat flux as the dominant factors generating these anomalies. The oceanic interannual variations are explained in terms of enhanced oceanic convection resulting from anomalous Ekman pumping and anomalous heat fluxes, both operating in a standing pattern dominated by wavenumbers 2 and 3.

1. Introduction

The Southern Ocean is an important element of the global climate system. The unique absence of blocking continents allows the Antarctic Circumpolar Current (ACC) to exchange water masses between the world's main ocean basins, muting interbasin differences caused by atmosphere–ocean interaction or other causes. Furthermore, the Southern Ocean plays a crucial role in the thermohaline circulation. North Atlantic Deep Water is injected into the Circumpolar Deep Water. Exposure to polar atmospheric conditions converts this water to either lighter surface water or denser cold water that sinks over the ocean bottom.

In past decades, progress has been made in our understanding of the ACC. Observations made in the framework of the International Southern Ocean Studies (ISOS) in the 1970s, the more recent World Ocean Circulation Experiment (WOCE) hydrographic sections, and observations made with satellite altimeters have contributed to our empirical knowledge. Insight into the dynamics of the ACC was greatly enhanced by the development of the Fine-Resolution Antarctic Model (FRAM) [Webb et al., 1991]. Nevertheless, many questions remain concerning the variability of the Southern Ocean climate. In this paper we try to answer some of

these questions by studying the response of an ocean general circulation model (OGCM) to the forcing with fluxes derived from the European Centre for Medium–Range Weather Forecasts (ECMWF) atmospheric reanalysis (ERA) [Gibson et al., 1996].

White and Peterson [1996] analysed 1985-1994 sea level pressure p_0, sea surface temperature T_0, meridional wind stress τ_y, and sea ice extent. Their data sets consisted of ECMWF operational analyses for p_0 and τ_y, in situ and satellite radiometer measurements for T_0, and sea ice extent. It should be noted that in all cases the actual number of observations is low, so that model dynamics and interpolation methods may have had a substantial impact. In any case, White and Peterson [1996] discovered a dominant signal of interannual variability, which they called the Antarctic Circumpolar Wave (ACW). It consists of anomalies in all four variables, propagating in a phase-locked manner. At a fixed location the signal repeats itself every 4-5 years, and the anomalies propagate eastward around Antarctica with an average velocity of about 8 cm/s. At about the same time Jacobs and Mitchell [1996] found TOPEX/POSEIDON altimeter measurements of anomalous sea surface heights ζ to be consistent with the ACW mode of White and Peterson [1996].

Climate variability may have different causes. Some variability is the result of internal variability of the atmosphere. In the extratropics this may originate from instabilities in the midlatitude atmospheric circulation, but it can also come from teleconnections with tropical

regions. In these cases the variability in the ocean is merely a response to the variability in the forcing air-sea fluxes, and the effect of the ocean on the atmosphere is unimportant. Other variability is related to interaction in the coupled atmosphere–ocean (–ice) system. In these cases, feedback from the ocean to the atmosphere is essential.

Several studies have tried to understand the nature of the ACW. So far, evidence is conflicting. A striking feature in the work of *White and Peterson* [1996] is the phase locking of the anomalies. This phase locking of, e.g., T_0 and p_0 variability supports a coupled explanation of the ACW. *White and Peterson* [1996], however, did not elaborate such an explanation, but suggested a teleconnection with the El Niño-Southern Oscillation (ENSO) phenomenon [*Karoly*, 1989]. *Qiu and Jin* [1997] have explored the ACW in their work as a genuine coupled mode. They did this on the basis of simulations with a simple atmosphere–ocean model. In these simulations the atmosphere promptly reacts to a positive T_0 anomaly with a high (low) p_0 anomaly to the east (west) of it. The corresponding wind stress anomalies deepen (shallow) the ocean mixed layer by Ekman pumping and the warm T_0 anomaly is strengthened by a warm geostrophic flow from the north [see *Qiu and Jin*, 1997, Plate 2]. In a similar way a cold T_0 anomaly is strengthened by a cold geostrophic flow from the south. Finally, the whole anomaly system is advected with the ACC: the pressure anomaly is phase-locked to the T_0 anomaly moving in the ACC.

Other modeling studies cast doubt on a coupled interpretation of the ACW. *Christoph et al.* [1998] have described the ACW mode from a long simulation run with a coupled GCM. Their ACW mode was confined to the east Indian and Pacific Oceans and the p_0 anomalies had the nature of a standing oscillation. More recently, *Weisse et al.* [1999] stochastically forced the Hamburg large-scale geostrophic (LSG) OGCM [*Maier-Reimer et al.*, 1993] with the surface fluxes derived from an Atmospheric Model Intercomparison Project (AMIP) run with the ECHAM3 model, an atmospheric general circulation model developed at the Max Plank Institut für Meteorologie in Hamburg [*Arpe et al.*, 1993]. Weisse et al.'s runs showed that the model ocean is able to integrate the atmospheric fluctuations to generate ACW-like patterns in the ocean surface layers, without the need of an ocean–atmosphere feedback.

In this study we have used the ECMWF reanalysis to analyze the atmospheric features of the ACW and we have forced the LSG model with the monthly surface fluxes of ERA. The ERA period (January 1979 to February 1994) overlaps the period considered by *White and Peterson* [1996] and extends it with the years 1979 to 1985. An important question is how robust the results of *White and Peterson* [1996] are when longer periods are considered. Their period of analysis contains only two instances of the mode. Remarkably, we find their T_0 signal throughout the ERA period, but in the

p_0 variability there exist two regimes. In particular, the phase locking between the T_0 and p_0 signal is absent over the period 1979 to 1984. This suggests that the dominant interannual variability may be a coupled mode only at certain times, while it is an uncoupled mode at other times. To resolve this issue, one would need to make long simulations with a coupled model, in which one can study both the influence of the ocean on the atmosphere and the influence of the atmosphere on the ocean. In the present study we have concentrated on the second half of the problem. Specifically, we have addressed the following questions: (1) what is the nature of the interannual variability of the ocean when it is forced by the atmosphere? (2) what is the dominant forcing mechanism?

To study, in deterministic detail, the oceanic response to a variable atmosphere, we performed a hindcast over the ERA period. The forcing fields are characterized by a pronounced interannual variability. The resulting patterns of interannual variability in the subsurface salinity and temperature will be identified. In addition, we have made a long (500 year) run in which the ocean was forced stochastically [*Hasselmann*, 1976]. The stochastic forcing was derived from the ERA surface fluxes. The record we obtain in this way is long enough to allow statistical treatment. We apply a principal oscillation pattern (POP) analysis, study the properties of a strong interannual ACW-like signal, and compare our results with those of *Weisse et al.* [1999].

Finally, we have made sensitivity studies to find out which physical air-sea exchange processes contribute to the generation of the ocean mode. This is done by selectively switching off the monthly variability in the forcing components: wind stress, heat, and freshwater flux. We will see that both dynamics (Ekman pumping) and thermodynamics (heat flux) play an important role.

The plan of this paper is as follows. We first describe the ERA data set and analyze its interannual variability in the region of the ACC. This is followed by a description of the LSG model and the way in which it is forced and initialized. The following two sections describe the analysis of the hindcast and the stochastic run. In section 6 we discuss the forcing mechanisms and the sensitivity experiments. Our conclusions are summarized in section 7.

2. Atmospheric Variability in ERA

The ECMWF reanalysis project [*Gibson et al.*, 1996] produced a consistent set of atmospheric data for the period from January 1979 to February 1994. The reanalysis was made with ECMWF's forecast and data assimilation system as it was operational in 1995. In this way a consistent treatment of the observations was achieved. The horizontal resolution of the data we analyzed equals $3° \times 3°$. We have used the data set to study its patterns of interannual variability. To this end we first determined the mean annual cycle of the ERA sur-

face fluxes: for each calendar month the average over the 15-year period was computed. For each individual month the anomaly is then defined as the average over that particular month minus the 15 year average for that same month. We will use the following notation

$$s = \bar{s} + s'. \qquad (1)$$

Here s is generic for fluxes and other fields. Quantities with an overbar are averages depending on the calendar month only. The anomalies s' depend on month and year. Apart from the ERA data set we will also consider other data sets. When confusion is possible we will use subscripts to distinguish between different data sets.

A first question is whether the ERA fields contain ACW-type signals. We investigated this by computing meridional averages between 46°S and 60°S of p_0 and T_0. These averages are band-pass filtered for timescales between 1 and 7 years. The results are given in the form of Hovmöller diagrams (Figure 1). Figure 1a for p_0 shows two different regimes. In the period 1985 to 1994 an eastward propagation occurs. In great contrast, the years before 1985 are characterized by a standing oscillation. There are no indications for an inhomogeneity in the observations used for ERA. Therefore we will assume that this two-regime structure is realistic.

The period 1985 to 1994 coincides with the period studied by *White and Peterson* [1996]. For this period our results are in close agreement with theirs. Apparently, eastward propagation is present in more or less the same way in the operational analysis used by *White and Peterson* [1996] and in the reanalysis used by us. The standing oscillation found in the earlier period 1979 to 1984 is qualitatively very different. The absence of an eastward propagation before 1985 is also found in the band-pass-filtered τ_y anomalies (not shown). Apparently, the atmosphere behaved rather differently in two different periods. It is interesting to note that the coupled model simulations of *Christoph et al.* [1998] also showed alternating periods of standing and propagating anomalies.

When we turn our attention to the ERA T_0 anomalies, we do not see such a pronounced difference. Figure 1b shows eastward anomaly propagation throughout the ERA period. This means that the period 1979 to 1985 has propagating T_0 anomalies that are not accompanied by propagating p_0 anomalies. This breakdown of phase locking suggests that atmospheric adjustment was weak. It casts doubt on the coupled nature of the observed variability. The average speed of the eastward propagation of the phase locked anomalies (6-8 cm/s) approximates the value found by *White and Peterson*
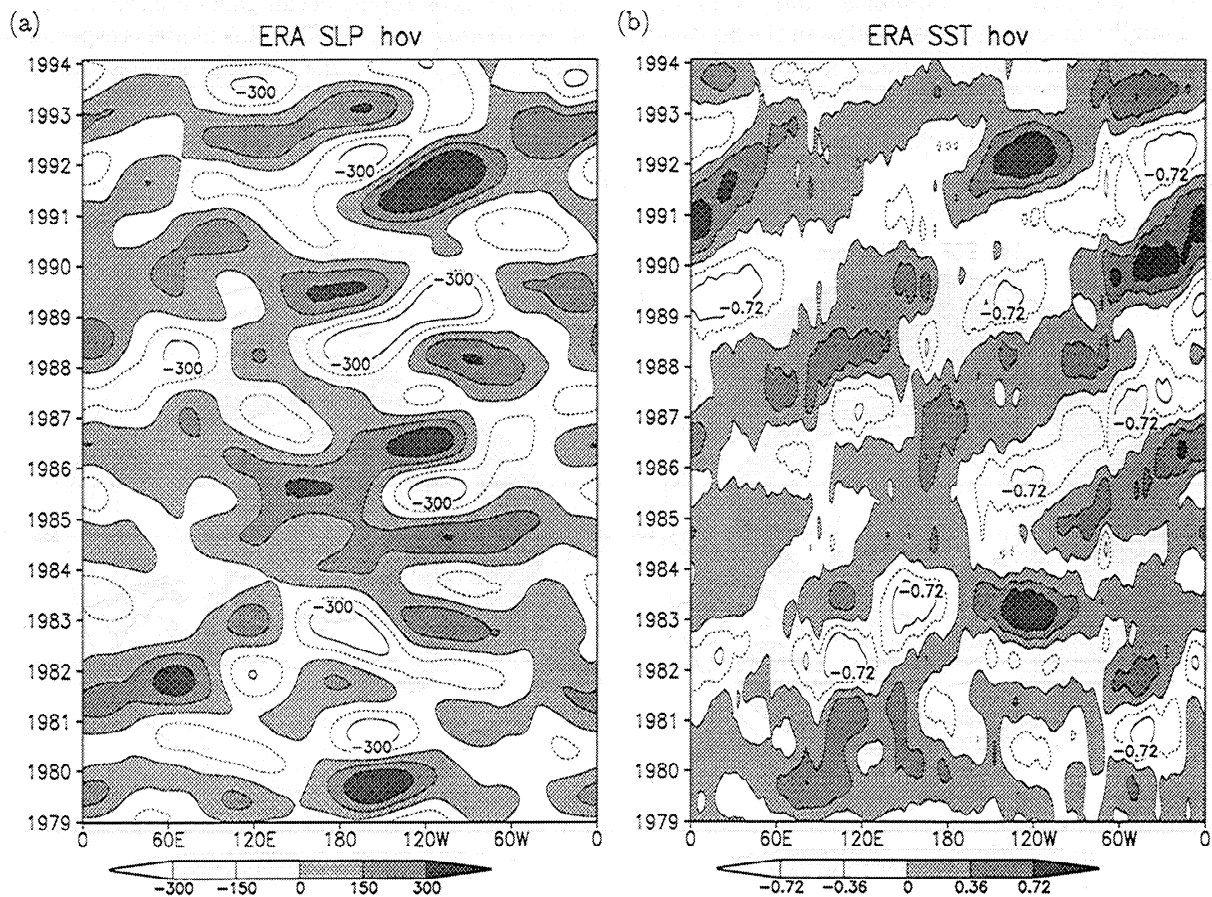

Figure 1. Hovmöller diagram of (a) European Centre for Medium–Range Weather Forecasts reanalysis (ERA) sea level pressure p_0 anomalies (hPa) and (b) ERA sea surface temperature T_0 anomalies (K) averaged over 48°S-60°S. Data are band-pass filtered (1–7 years).

[1996] and is roughly equal to the surface velocity of the ACC. Figure 1 and an empirical orthogonal function (EOF) analysis (not shown) of the band-pass-filtered anomalies reveal another feature of the ERA ACW signal: The strongest anomalies, in particular those of p_0, are found in the Pacific Ocean. In the model study of *Christoph et al.* [1998], high amplitudes were also confined to the Pacific Ocean.

So far, we have studied the band-passed anomalies. However, our goal to study the variability in the ocean response requires an analysis of the whole spectrum of atmospheric variability and its spatial characteristics, because we know that inertia of the ocean can transform white noise forcing into a low-frequency response [*Hasselmann*, 1976]. From an analysis of the local variances we have found that the band-pass-filtered anomalies described above (Figure 1a) contain only a limited fraction of the total variability. This fraction seldomly exceeds 20%. Therefore it is certainly not obvious that the low frequency signals in the ocean are determined by the low frequencies in the atmospheric forcing.

To address the spatial characteristics of the complete atmospheric variability, we have computed empirical orthogonal functions of the ERA p_0 variability. The result for the first EOF of the p_0 anomalies, shown in Figure 2a, reveals a striking wavenumber 3 domination. A similar pattern was found by *Connolley* [1997], who analyzed variability in annually averaged p_0 in the Southern Ocean. He also found that in model generated p_0 this

fixed pattern is rather insensitive to variations in the prescribed surface temperature. In a spectral analysis of the coefficient of the first EOF of p_0 variability we have found no preferred timescale of variability. Thus, for the pattern of this EOF, the p_0 variability nearly equals white noise. For later reference we have also computed the first EOF of the wind stress curl $\nabla \times \tau$, which determines the strength of the Ekman pumping. The result is shown in Figure 2b. The corresponding time series also has the white noise characteristics of the first EOF of p_0 variability.

The spatial wavenumber 3 pattern and the white noise behavior of the first EOF of p_0 and wind stress curl form important ingredients of the atmospheric forcing, which can determine a low frequency (ACW like) response in the ocean. This has been illustrated by *Weisse et al.* [1999] in their study of the response of a simple ocean advection model forced by atmospheric white noise with a pure spatial wavenumber 3 pattern. The low-frequency response to the ERA forcing is the subject of the next sections.

3. OGCM Spin Up and Forcing

The global ocean model used for the oceanic hindcast and stochastically forced runs is the Hamburg large scale geostrophic ocean general circulation model [*Maier-Reimer et al.*, 1993]. This model is especially designed for long-term climate change studies. Its concept
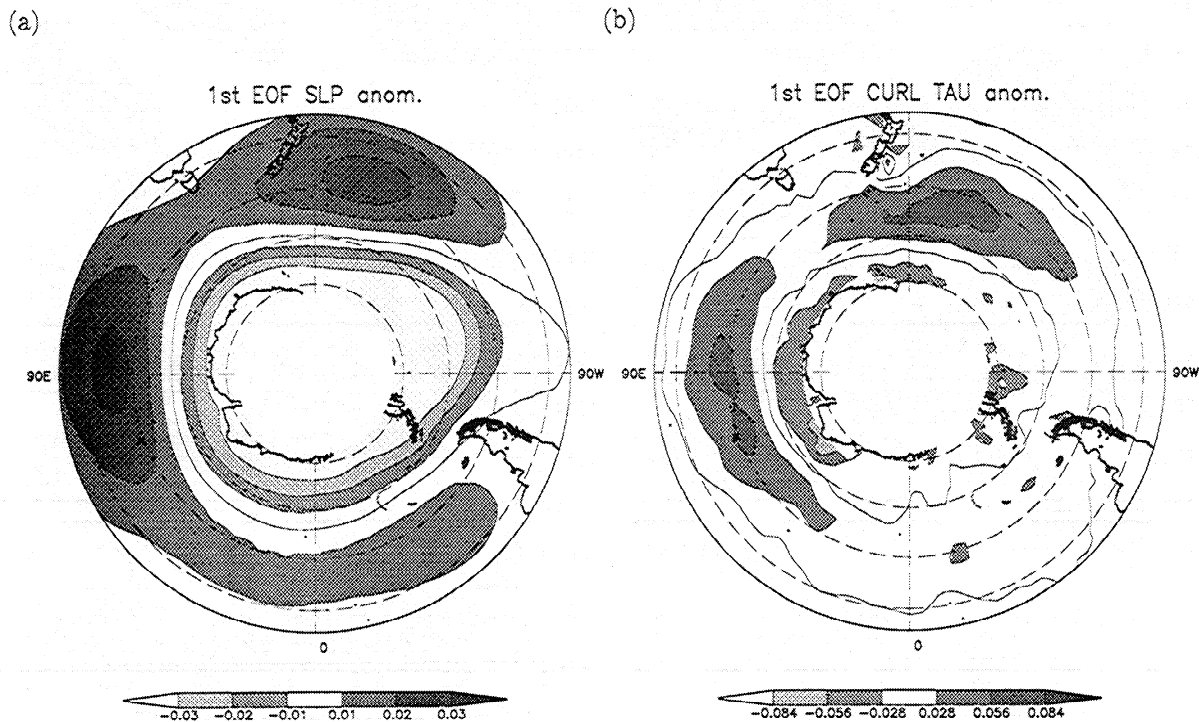
(a)   (b)

Figure 2. First empirical orthogonal function (EOF) of (a) p_0 anomalies and (b) wind stress curl $\nabla \times \tau$ anomalies. The EOFs explain 19% and 18% for p_0 and $\nabla \times \tau$, respectively, of the total variance.

is based on the observation that spatial scales smaller than the internal Rossby radius and timescales smaller than the periods of the gravity modes and barotropic Rossby waves can be omitted for the study of long-term climate variability. Technically, the small and fast scales are filtered out by neglecting the nonlinear advection terms of momentum in the full primitive equations. The effective horizontal resolution of the model equals 3.5°. In the vertical, 11 levels are used, which are centered around the depths of respectively 25, 75, 150, 250, 450, 700, 1000, 2000, 3000, 4000 and 5000 m, respectively. A realistic bottom topography and a simple thermodynamic ice model are included. The strength of the convection is measured in terms of the work done by the buoyancy force in each time step.

The implicit time integration of the LSG model allows a time step of 1 month. *Maier-Reimer et al.* [1993] argued that monthly averaged forcings fail to capture strong ocean-to-atmosphere heat fluxes originating from shorter-timescale processes (e.g., cold air outbreaks). To overcome this problem, the subtimescale processes are parameterized by introducing an effective air temperature T_{eff}. This temperature is defined by a simple atmospheric advection equation,

$$\frac{\partial T_{eff}}{\partial t} + \mathbf{v} \cdot \nabla T_{eff} = \frac{T_{eff} - T_{air}}{t_c}, \qquad (2)$$

which is solved for every time step and relates the effective temperature to the monthly averaged air temperature T_{air}. The near-surface winds are denoted by $\mathbf{v}$, and the characteristic timescale t_c is set to approximately 1/2 month. The effect of this equation is that upwind temperature gradients modify the effective air temperature.

Before we can study the variability in the ocean model in response to the surface flux variability, we must adjust the mean ocean model state to be in equilibrium with the ERA flux data and we must correct the forcing heat and freshwater climatologies for the application of mixed boundary conditions. This is done with a two-stage spin up procedure. First, the 5000 year spin-up as described by *Maier-Reimer et al.* [1993] is extended with a 1000 year run. In this run the ERA wind climatology $\bar{\tau}_{ERA}$ is applied under restoring conditions. The salinity and temperature of the first layer S_{25} are respectively relaxed toward the *Levitus* [1982] sea surface salinity climatology $S_{lev,0}$ and the effective air temperature $\bar{T}_{eff}$, which is computed by solving (2) with $\mathbf{v} = \bar{\mathbf{v}}_{ERA}$ and $T_{air} = \bar{T}_{ERA,air}$. This leads to the following heat flux:

$$Q_1 = \lambda_1 (\bar{T}_{eff} - T_{25}) \qquad (3)$$

with relaxation coefficient $\lambda_1 = 40 \text{ W/m}^2\text{K}$. Second, to reach a quasi-stationary state under mixed boundary conditions, we have made two additional 1000 year runs: In these runs we used the freshwater flux as diagnosed from the last 100 years of the run with restoring conditions, $H = \bar{H}^{diag}$. The heat flux is determined in

an iterative way. In each new run $(n + 1)$ the heat flux Q_n^{diag} is diagnosed from the last 100 years of the previous run n: We still relax to $\bar{T}_{eff}$, but with a smaller relaxation coefficient $\lambda_2 = 16 \text{ W/m}^2\text{K}$. In this way the forcing heat flux becomes

$$Q_{n+1} = \bar{Q}_n^{diag} + \lambda_2 (\bar{T}_{eff} - T_{25}) \qquad (4)$$

The ocean fields so obtained are used to initialize the experiments described below. The differences between, on the one hand, the diagnosed heat flux $\bar{Q}^{diag} = \bar{Q}_3^{diag}$ and freshwater flux $\bar{H}^{diag}$ climatologies and, on the other hand, the corresponding ERA flux climatologies act as flux corrections.

Two types of run are performed, hindcast runs and stochastic runs. In either case the following forcing was applied:

$$\tau = \tau_{ERA} = \bar{\tau}_{ERA} + \tau'_{ERA} \qquad (5)$$
$$H = \bar{H}^{diag} + H'_{ERA} \qquad (6)$$
$$Q = \bar{Q}^{diag} + Q'_{ERA} + \lambda_2 (\hat{T}_{eff} - T_{25}). \qquad (7)$$

We still require a relaxation term to stabilize the model simulation. Its justification follows the usual argument. In reality a small fluctuation in ocean temperature is damped by a modification of the heat flux. In forced ocean runs this is simulated by the relaxation term. As in the spin-up, we relax to an effective air temperature, $\hat{T}_{eff}$, which accounts for high-frequency temperature fluctuations. This $\hat{T}_{eff}$ is obtained by solving (2) with $\mathbf{v} = \mathbf{v}_{ERA}$ and $T_{air} = \bar{T}_{ERA,air}$.

In the hindcast run (182 months) the flux anomalies of ERA are used sequentially. In the stochastic runs (500 years) they are chosen as follows: the January anomaly is randomly chosen from the 16 ERA January anomalies, the February anomaly from the 16 ERA February anomalies, etc. This procedure (identical to the one used by *Weisse et al.* [1999]) creates longer time series, enabling a statistically robust treatment. The same month is chosen for all the forcing components to maintain their natural coherence.

We have also made runs with the forcings used by *Weisse et al.* [1999]. Their forcing climatology is based on *Hellerman and Rosenstein* [1983] τ, $S_{lev,0}$ and Comprehensive Ocean–Atmosphere Data Set (COADS) T_{air} [*Woodruff et al.*, 1987]. These fields were used to produce the surface fluxes and spin-up state in a manner similar to the spin-up described above. Their monthly anomalies were derived from AMIP simulations with the ECHAM-T42 atmospheric GCM (AGCM) [*Arpe et al.*, 1993].

Table 1 gives an overview of the runs we performed. To distinguish between the different runs, we will use a shorthand nomenclature, for example, the stochastic run with the ERA climatology and AMIP anomalies is denoted as ERA+AMIP.

In the basic hindcast and stochastic runs the monthly anomalies of all the components are taken into account.

Table 1. Large-Scale Geostrophic Model Runs Made With Different Forcings

Climatology	Anomaly	
	ERA	AMIP
ERA	hindcast, stochastic	stochastic
HR	stochastic	stochastic

Climatology acronyms (ERA, European Centre for Medium-Range Weather Forecasts reanalysis, and HR *Hellerman and Rosenstein* [1983]) also refer to the spin-up state and the diagnosed heat flux Q and H. AMIP is Atmospheric Model Intercomparison Project.

To analyze the sensitivity with respect to the individual forcing components (τ, Q, and H), we made additional sensitivity runs in which we systematically neglect the anomalies of individual components. These runs will be discussed in more detail in section 6.

4. Hindcast of Interannual Ocean Variability

To study the oceanic response to the observed variations in the atmosphere (see section 2) we have made a hindcast run with the LSG model for the full ERA period (i.e., January 1979 to February 1994). In our analysis we looked in some detail at the interannual variability in temperature and salinity of the 25, 75, 150, 250, and 450 m layers, in sea surface elevation ζ and in convection C (see section 3).

The basic run is defined with the forcing described in (7). A striking feature is a low-frequency (decadal) zonally symmetric variation of the surface salinity. This signal turned out to be related to a slow zonally symmetric variation in the ERA freshwater flux. Since we are primarily interested in the ACW-type patterns, we have taken out this signal by neglecting the freshwater fluctuations. So the results presented in the remaining part of this section were obtained with $H = H^{\mathrm{diag}}$.

We first discuss the temperature and salinity variability in the 75 m layer. Figure 3 contains Hovmöller diagrams of the salinity and temperature anomalies. Both diagrams show an eastward propagation of persisting anomalies in a zonal band between 46°S and 61°S. At a fixed location the anomalies reappear every 4 to 5 years. Strong anomalies originate from around 180°W, and the highest amplitudes are found in the east Pacific (130°W - 100°W). These patterns are in agreement with the results of the stochastic run (see section 5, e.g., Fig-
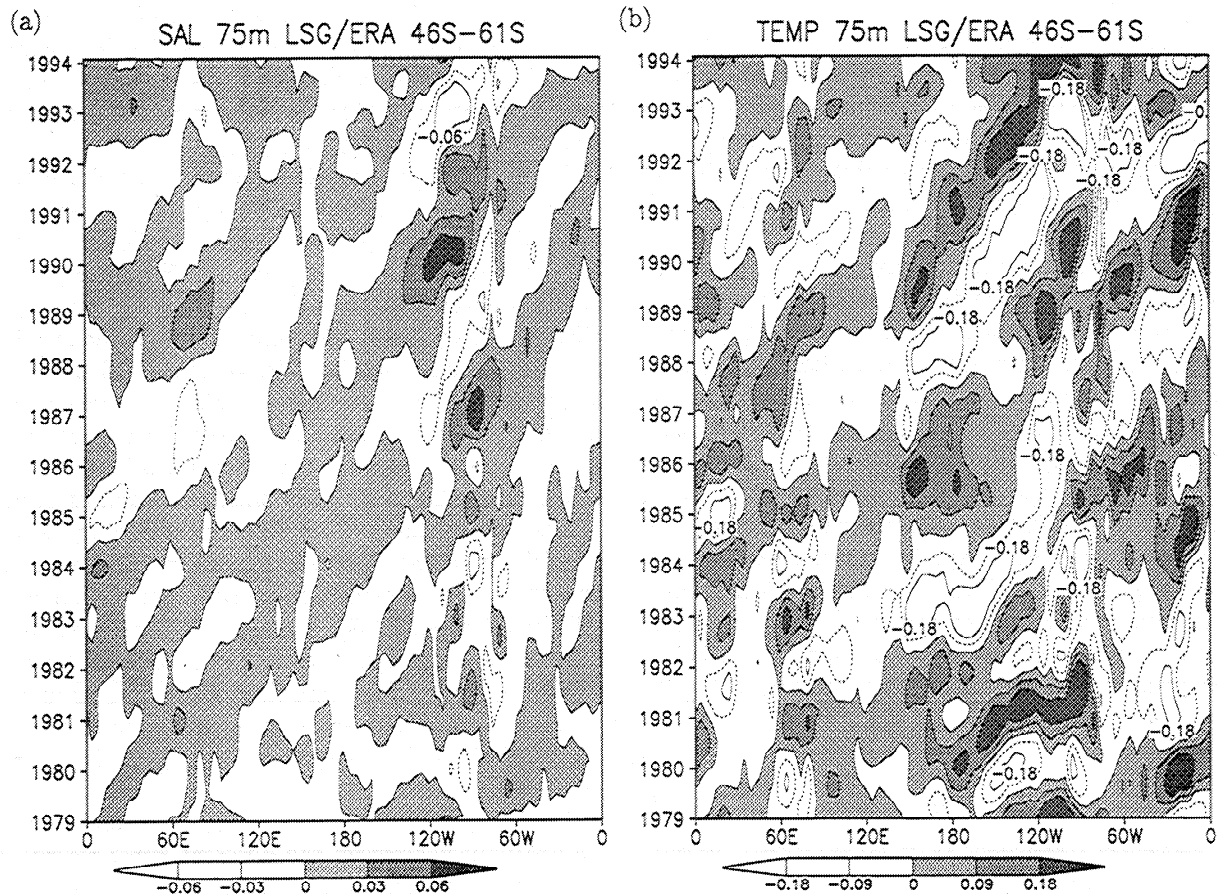

Figure 3. Hovmöller diagram of (a) salinity (ppt) and (b) temperature (K) anomalies in the 75 m layer. The anomalies are averaged over 46°S-61°S and band-pass filtered (1-7 years). The plots are based on a run in which freshwater flux variability is neglected.

ure 6). More moderate anomalies appear in the Indian Ocean (65°-75°E).

Next we compare the results of the 75 m layer with the atmospheric ACW patterns found in the ERA data set (see section 2). The oceanic response resembles the two-regime structure of the p_0 variability in the sense that stronger anomalies and a more pronounced eastward propagation are present in the period of 1985 to 1994 (see Figure 3). However, the oceanic anomalies travel considerably slower than the atmospheric anomalies. We can explain this by a comparison of the LSG surface velocity fields with the more realistic velocity fields of FRAM [Webb et al., 1991]. FRAM produces surface velocities roughly twice as large when forced with the Hellerman and Rosenstein [1983] (HR) climatology. So despite a reasonably realisitically averaged Drake Passage transport ($\approx$125 Sv), the LSG model produces a local advection that is too weak. This paradoxical result is due to the coarse resolution of the model in which Drake Passage is too wide. Assuming that the oceanic part of the ACW is strongly governed by advection and only weakly coupled to the atmosphere, we cannot expect the local phases of the interannual oceanic mode to be consistent with the ACW mode in the atmosphere. We will come back to this point in section 5.

The temperature and salinity results of the 75 m layer are illustrative for the other upper layers of 25, 150, 250 and 450 m. The 450 m results are shown in Figure 4 to illustrate this. In these layers we have found the same dominant oscillation period and the same patterns. Some differences are found in phase shifts and reduction of the amplitudes. For example, in the 450 m layer the signs of the strong temperature anomalies of the early 1990s near 120°W are reversed. This reversal is an indication of anomalous convection, which will be discussed in more detail in section 6. In the deeper ocean (e.g., the 700 m layer) the ACW like signal is recognizable but its amplitude is reduced.

We also looked at the variability in surface elevation ζ and convection C. Figure 5b depicts a Hovmöller diagram of ζ variability. For the periods 1986-1990 and 1992-1994 the anomaly patterns can qualitatively be identified with the TOPEX/POSEIDON altimeter measurements studied by Jacobs and Mitchell [1996, Plate 1], but propagation of the model ζ anomalies is slower than observed. This is one more consequence of the low surface velocities. Considering the complete ERA period, we observe a regime switch in ζ variability around 1985 similar to the one found in p_0. The cause for this regime switch is not understood. The output of anomalous C (Figure 5a) suggests a relationship be-
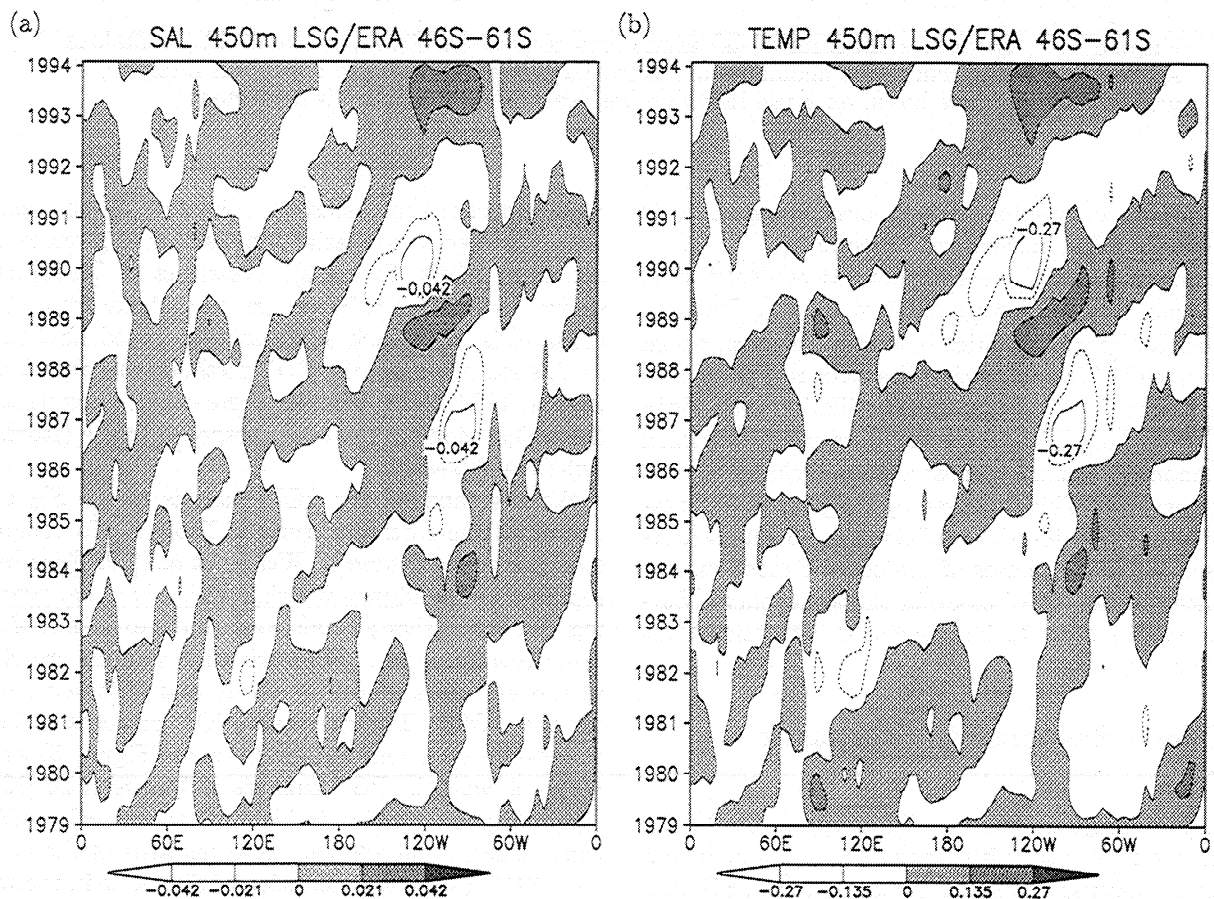

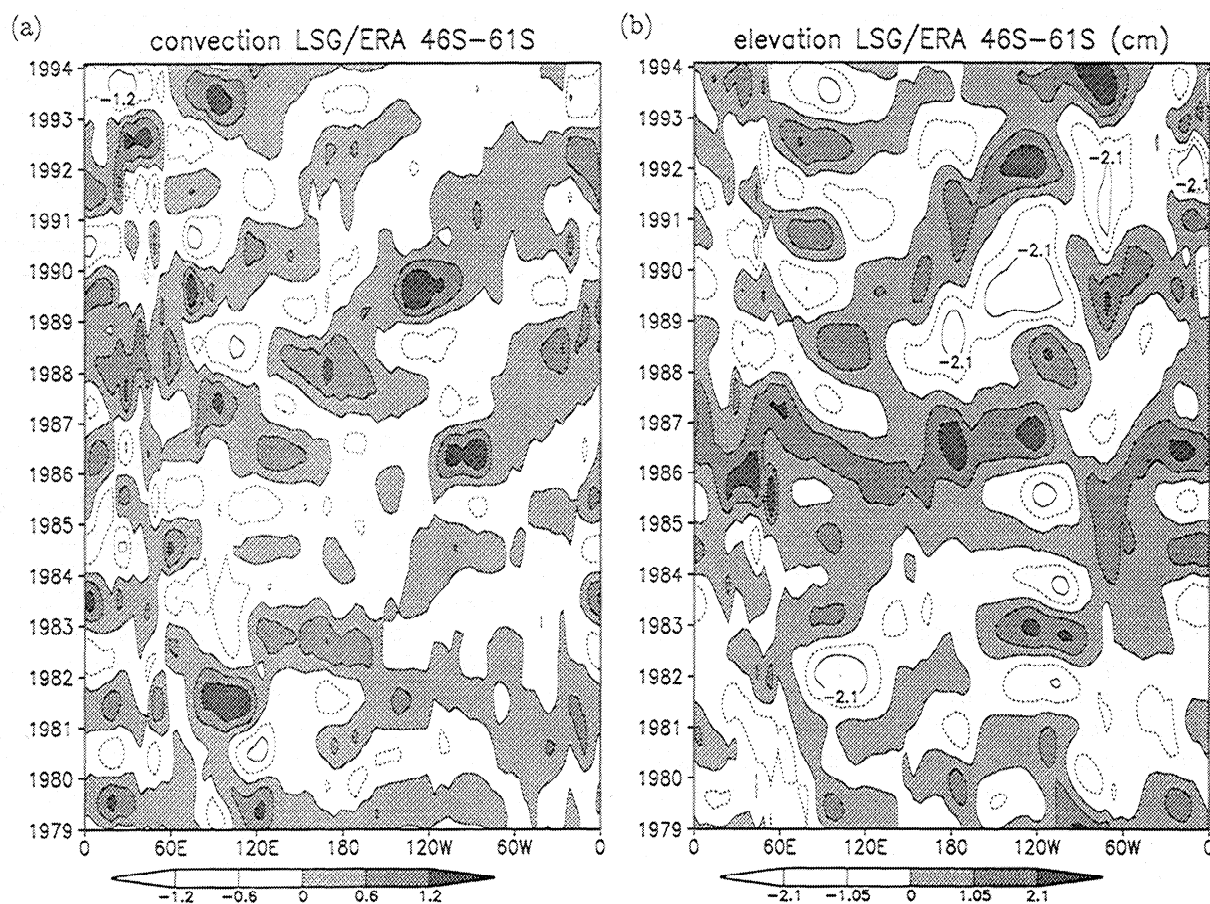Figure 4. Same as in Figure 3, but for the 450 m layer.

Figure 5. Hovmöller diagram of (a) anomalous convection C (W/m^2) and (b) anomalous surface elevation ζ (cm). The anomalies are averaged over 46°S-61°S and band-pass filtered (1-7 years). The plots are based on a run in which freshwater flux variability is neglected.

tween oceanic convection and the oceanic mode. This will be explored in more detail in section 6.

In summary, in the hindcast run we have identified an oceanic mode with a strong ACW signature. Evidence for the ACW characteristics is found in several ocean variables and different layers. The strongest anomalies are located in the Pacific, and the oscillation period is in the 4-5 year range. However, the eastward propagation of the anomaly signal is almost a factor 2 slower than in the atmosphere. This is caused by the poor representation of local velocities of the ACC in the LSG model. As a consequence, the phases of the oceanic mode cannot be related to the ACW mode in the atmosphere. Surface anomalies seem to be associated with anomalous oceanic convection.

5. Ocean Response to Stochastic Forcing

In the hindcast run we have identified an ACW-like oceanic mode of variability for the ERA period. In this section we discuss the stochastically forced LSG runs (see section 3), which allow us to study this mode in a statistically robust manner. The stochastically forced runs neglect the intraseasonal coherence of the anomalies but preserve the spatial organisation as given by the dominant EOFs (Figure 2). *Weisse et al.* [1999] have shown the existence of an interannual signal with ACW characteristics in their stochastically forced LSG runs. In this study we use the POP method [*von Storch and Zwiers*, 1997] to see whether there exists a comparable dynamical mode in the ocean response to the (stochastic) ERA fluxes.

We have applied the POP analysis to the S_{25} output of all the stochastic runs of Table 1. To compare our results with those of *Weisse et al.* [1999] we have replaced the band-pass filtering with an annual averaging. We found that all runs confirm the existence of the same oceanic mode. The oscillation periods are close to the 4-5 years found by *White and Peterson* [1996] for the ACW. The dominant POP patterns of both the ERA+ERA and HR+ERA runs (Figure 6) agree very well with the POP analysis of *Weisse et al.* [1999] (their Figure 1, which is identical to our HR+AMIP run). The spatial and temporal patterns of the dominant POP give us an excitation of the mode in the west Indian Ocean (70°E), a strong growth or a stronger excitation around 180°E, and a decay after Drake Passage.
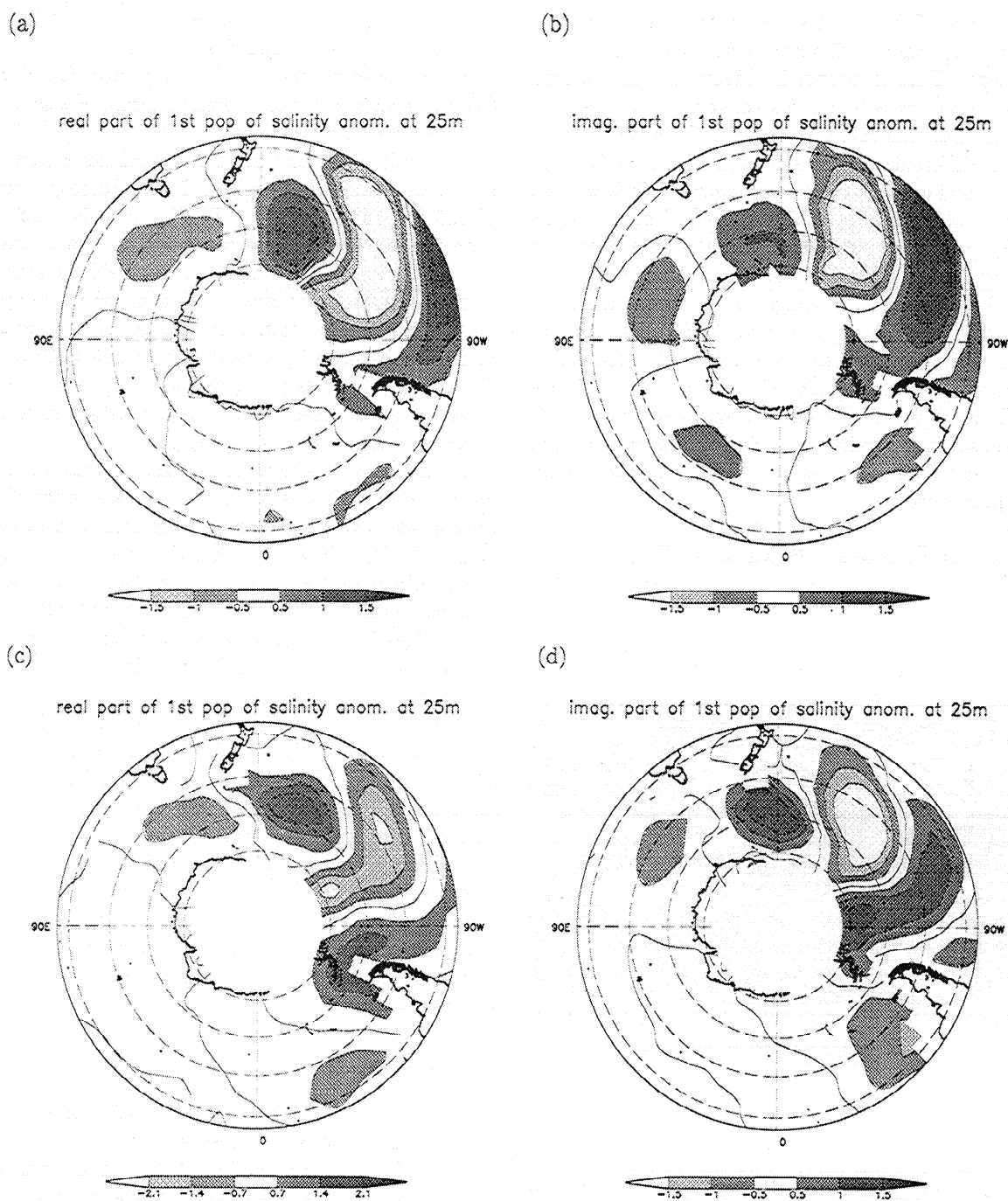
(a)

real part of 1st pop of salinity anom. at 25m

(b)

imag. part of 1st pop of salinity anom. at 25m

(c)

real part of 1st pop of salinity anom. at 25m

(d)

imag. part of 1st pop of salinity anom. at 25m

Figure 6.   The (a) real and (b) imaginary part of the dominant principal oscillation pattern (POP) of the sea surface salinity (25 m) anomalies of the ERA+ERA stochastic run and the (c) real and (d) imaginary part of the dominant POP of the sea surface salinity (25 m) anomalies of the HR+ERA stochastic run, explaining 19% (ERA+ERA) and 21% (HR+ERA) of the total variance. HR refers to *Hellerman and Rosenstein* [1983] climatology.

In all run, the variance locally explained by the POP exceeds 25% in the central part of the South Pacific Ocean. The patterns of locally explained variance (not shown) match those of *Weisse et al.* [1999].

Next we investigate the relation between the oscillation period and the eastward propagation in further detail. In general, the frequency spectrum of the ocean response is not only set by the variability in the ocean-

atmosphere fluxes but also by the mean advective response in the ocean (see, e.g., the recent work of *saravanan and McWilliams* [1998]). We believe that we have some evidence that the dominant (ACW like) timescale of the ocean response is fully determined by the velocity and length scales of the Southern Ocean basins. This evidence comes from a comparison of the ERA+ERA and the HR+ERA runs. It turns out

that the global ERA wind stress climatology has very marked (up to order 1) differences compared to the HR climatology. This is shown in Figure 7. In general, the ERA wind stress is much stronger over the Southern Ocean than the HR wind stress. This results in a significant difference in the strength of the ACC. Figure 8 shows the effect of the stronger ACC flow with ERA climatology for an arbitrary period of 100 years of the S_{25} response. The interannual signal shown in these Hovmöller diagrams is essentially described by the POPs of Figure 6. The propagation of the anomalies is faster with the ERA climatology. This in agreement with the notion of a passive advection with the ACC. Furthermore, the amplitude of these anomalies is reduced. This might also be caused by the stronger ACC in the sense that forcing mechanisms operate within shorter time periods. A passive advection of the anomalies would require

$$T_{\mathrm{ERA+ERA}} \, \overline{u}_{\mathrm{ERA+ERA}} = T_{\mathrm{HR+ERA}} \, \overline{u}_{\mathrm{HR+ERA}},$$
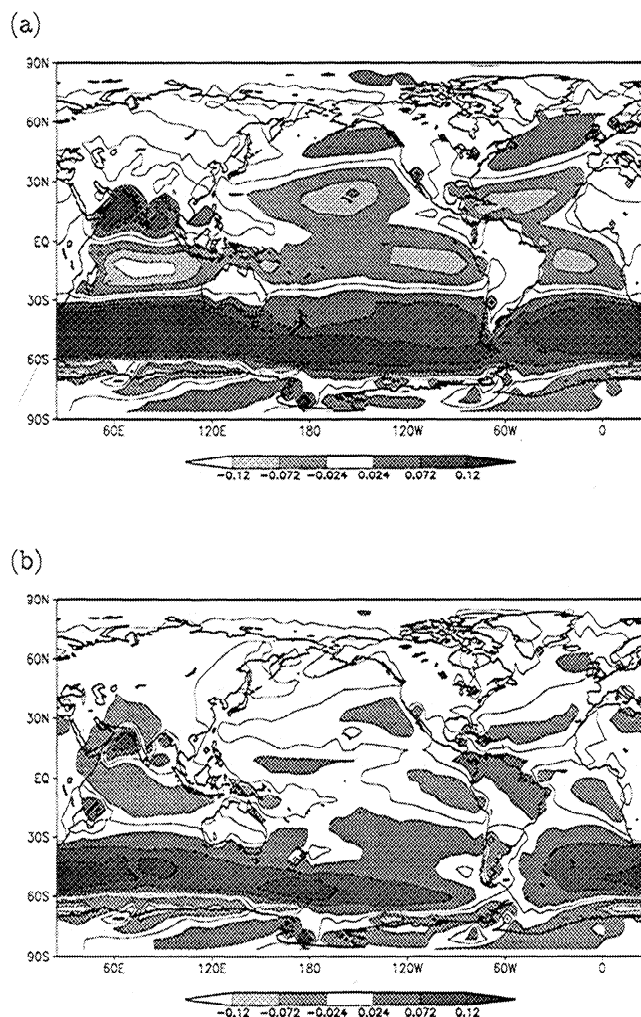

(a)

(b)

Figure 7.   Global zonal wind stress for (a) ERA climatology (Pa) and (b) showing differences with the HR climatology, ERA-HR (Pa).

in which T is the dominant oscillation period and $\overline{u}$ is a measure of the averaged strength of the ACC. We have set these to the oscillation period found by the POP analyzes and the averaged Drake Passage transport as present in the LSG model, respectively (which is proportional to the averaged local advection). The model produces an averaged Drake Passage transport of 125 Sv when forced by ERA, which is much larger than the 100 Sv when forced by HR. The corresponding oscillation periods found in the POPs equal 4.79 and 6.03 years, respectively. The latter value approximately equals that found by *Weisse et al.* [1999]. We find that the equality holds: $4.79 \times 125 \approx 6.03 \times 100$. This again supports the hypothesis that the ACW-type behavior in the ocean is set by passive advection of interannual anomalies by the ACC.

We have also made a comparison of runs with different anomalies. It was found that the statistics of AMIP anomalies have only small differences compared with those of ERA: The leading EOFs and the local root-mean-square values match. Consequently, the variabilities in the responses of the stochastic runs ERA+AMIP and HR+AMIP have only small differences compared with those of the ERA+ERA and HR+ERA runs, respectively.

The T_{25} anomaly patterns (not shown) follow those described by the S_{25} POPs but are somewhat noisier. The ACW characteristics are also present in the stochastically forced ocean temperature and salinity variability of the other upper layers.

In short, the stochastically forced runs confirm the robustness of the ACW-like oceanic mode as found in the hindcast run (section 4). In addition, the application of different forcing climatologies supports the determination of the dominant oscillation period by the advective velocity scale.

6. Forcing Mechanisms

In this section we consider the question of which physical air-sea exchange processes contribute to the generation of the ocean mode. A first clue comes from the observation that the oceanic mode observed in both temperature and salinity goes together with anomalous convection (Figure 5a). This inspired us to postulate that the air-sea transfer takes place in two steps. (1) Anomaly information from the atmosphere is passed to the ocean by anomalous surface fluxes. These flux anomalies are integrated by the ocean and eventually initiate anomalous convection. (2) Anomalous convection enhances anomalies in the surface and deeper layers of the ocean. These anomalies are then advected by the ACC, as was discussed in section 5, and maintained by the ongoing anomalous convection. We will now discuss the two steps.

Let us begin with the anomalous convection. The top and intermediate layers (up to 1000 m) of a considerable part of the Southern Ocean are known [*Webb et al.*,
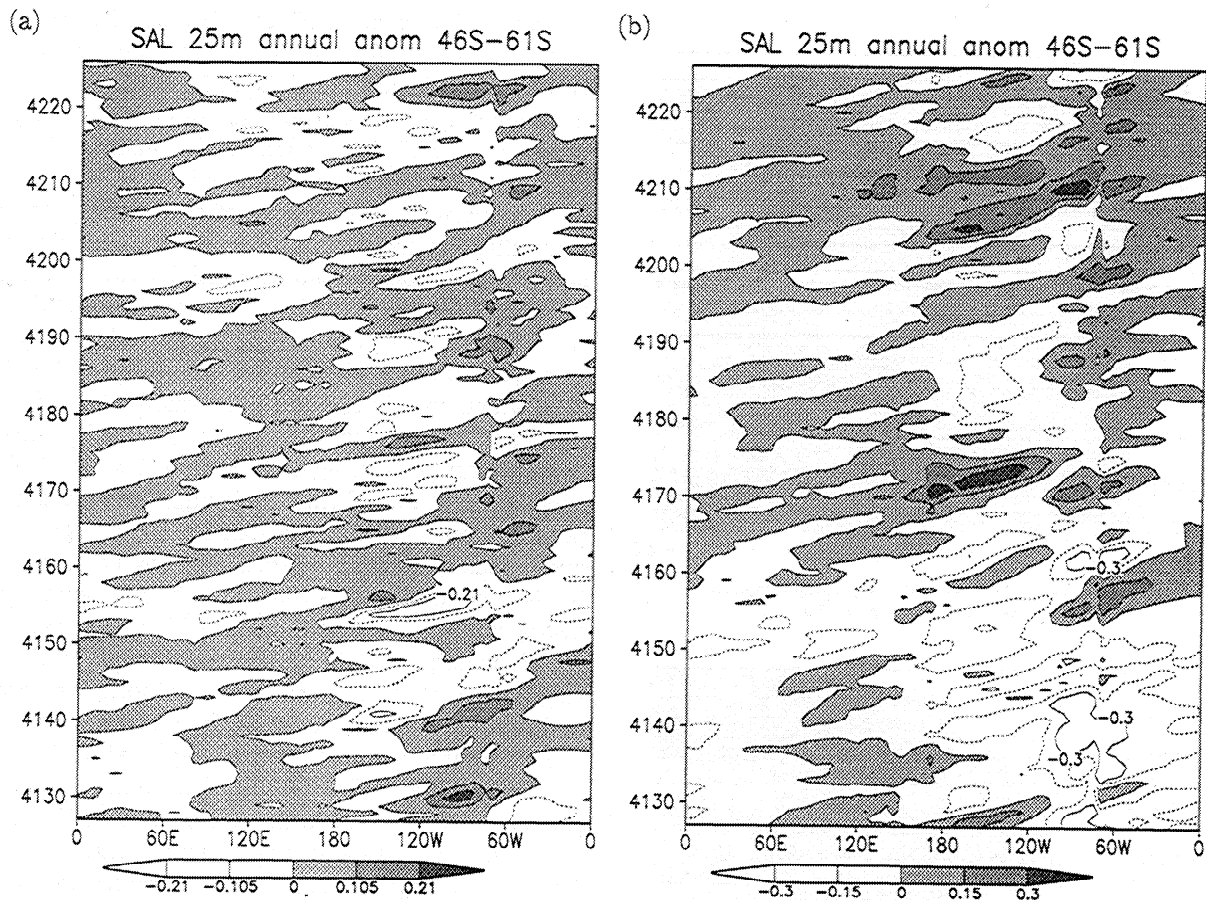
Figure 8. Hovmöller diagrams of annual salinity anomalies (ppt) at 25 m averaged over 46°S-61°S using (a) ERA climatology and (b) HR climatology. Both plots are for an arbitrary 100 years of the basic stochastic run. Note the different contouring.

1991] to be marginally stratified with relatively warm and saline waters masses flowing under the cool and freshwater at the surface. The marginal stratification is captured by the LSG model ocean (Figure 9) and qualitatively comparable to the stratification in the FRAM atlas [*Webb et al.*, 1991]. The warm and saline water of the deeper layers reaches the surface when convection is triggered. In the top layer the density of this water is increased by surface cooling and its sinking results in an even stronger convection. This positive feedback allows surface anomalies to be strengthened.

Once a surface anomaly exists, it is advected with the ACC. The circumpolar character of the marginal stratification allows convection all along the trajectory of these anomalies. In this way the anomalies can be maintained in time against the turbulent dissipation in the top layers.

Second, to address the initiation of the convection, we want to identify the dominant forcing flux anomalies. To this end we have performed sensitivity runs with the hindcast forcing. The sensitivity runs are defined by switching on or off the monthly variability in the three components of the forcing (τ, Q, and H). If all the anomalies are switched off, the quasi-stationary state of

the spin-up is prolonged and the ocean response does not contain any significant variability. On the other hand, in the case that all the anomalies are switched on, we have the basic hindcast run. An overview of the various sensitivity runs is given in Table 2.

Figure 10 shows the results of the sensitivity runs for ocean temperature and salinity in terms of a wavenumber-frequency decomposition. With this decomposition we can represent the spatial patterns and dominant oscillation frequency (previously depicted in EOFs and Hovmöller diagrams, respectivley) in a synoptic manner. The amplitude squared of a mode with spatial wavenumber k and frequency ω is given by

$$A^2(k,\omega) = (A_c^2 + A_s^2)/n^2 m^2$$

with

$$\begin{aligned}
A_c(k,\omega) &= \sum_{i=0}^{n} \sum_{j=0}^{m} s'(x_i, t_j) \cos[\phi_{ij}(k,\omega)], \\
A_s(k,\omega) &= \sum_{i=0}^{n} \sum_{j=0}^{m} s'(x_i, t_j) \sin[\phi_{ij}(k,\omega)], \\
\phi_{ij}(k,\omega) &= 2\pi(ki/n - \omega j/m),
\end{aligned}$$

in which n and m are determined by the spatial and temporal resolution. A wavenumber-frequency decomposition is made for the 75 150, 250, and 450 m layers.
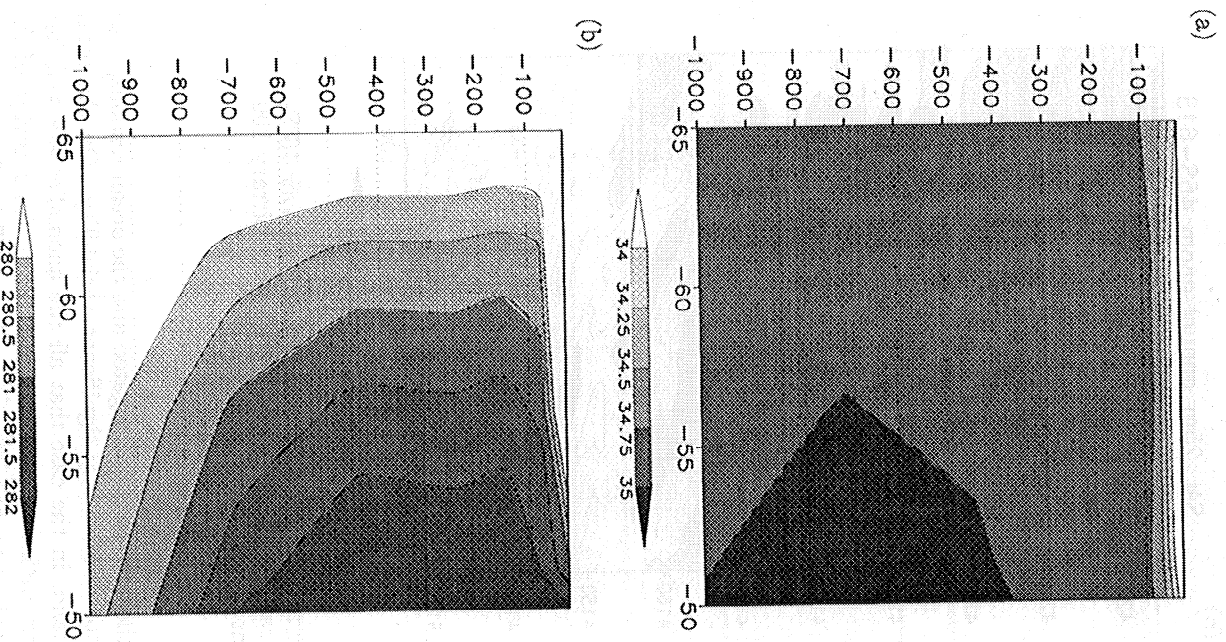
(a)

(b)

Figure 9. Meridional crossection of the Southern Ocean at 90°W. showing (a) salinity (ppt) and (b) temperature (K).

Table 2. Sensitivity Runs

	Variability			Figure 10
Run	τ	Q	H	Panels
Basic	on	on	on	a, b
No H anomalies	on	on	off	c, d
Dynamic forcing	on	off	off	e, f
Thermodynamic forcing	off	on	off	g, h

Variables are defined as follows: τ, wind stress; Q, heat flux; and H, freshwater flux.

We have analyzed the decomposition results of the individual layer. In Figure 10 we present the squared amplitudes averaged over these four layers.

Figures 10a and 10b show the temperature and salinity variability, respectively, of the basic run (see also Figure 3). In both Figures 10a and 10b, high amplitudes are found for the ACW characteristics consisting of a spatial wavenumber 2-3 pattern and a frequency of ≈ 0.2 cycles per year. The salinity figure contains also a wavenumber 4-5 pattern. We have not analyzed this pattern in detail. It is absent in the deeper layers.

The H variability hardly contributes to the generation of the oceanic mode. This can be inferred from the small differences of Figures 10c and 10d compared with to Figures 10a and 10b. The main effect of the H variability is additional noise in the 25 m layer and (consequently) the ζ output (not shown). At this point, Q and τ variabilities remain as the main forcing components of the oceanic interannual variability.

To analyze the importance of either the τ or the Q variability, we have made a sensitivity run with a dynamic surface forcing and a sensitivity run with a thermodynamic surface forcing, respectively. In the first run we have also excluded the surface wind variability from the subtimescale parameterization ($v = \bar{v}_{ERA}$; see (2)), which contributes to the thermodynamic forcing.

When compared to the previous sensitivity runs, the dynamic surface forcing case (Figures 10e and 10f) features a reduction of the amplitudes of both the temperature and salinity variabilities. The strength of anomalous convection, as measured by C (not shown) is also reduced in this case, but it has certainly not disappeared. The peak values still correspond to an ACW pattern. In short, the ACW characteristics of the oceanic mode are preserved for both temperature and salinity in the dynamic surface forcing case.

The oceanic mode is less well captured with a solely thermodynamic surface forcing. The temperature number-frequency spectrum still contain ACW characteristics, though in a strongly reduced fashion (Figure 10g). For salinity the ACW characteristics have almost disappeared (Figure 10h). In anomalous convection the ACW signal is still present (not shown) but, again, amplitudes are reduced.

In brief, the sensitivity studies have shown that the dynamic forcing associated with τ variability is dominant in generating the ocean ACW mode. A solely thermodynamic forcing is also able to produce this mode, though in a reduced fashion.

Next we discuss some physical interpretations of the two convection triggering mechanisms. In this discussion we put an emphasis on the fixed spatial organisation of the atmospheric variability as described by the first EOF of the p_0 anomalies (Figure 2a). First, in the dynamic forcing case, anomalous Ekman pumping (most strongly present in the Indian and west Pacific Oceans; see Figure 2b) brings warm subsurface water to the surface. In this process the stratification is further reduced and normal surface cooling can start oceanic
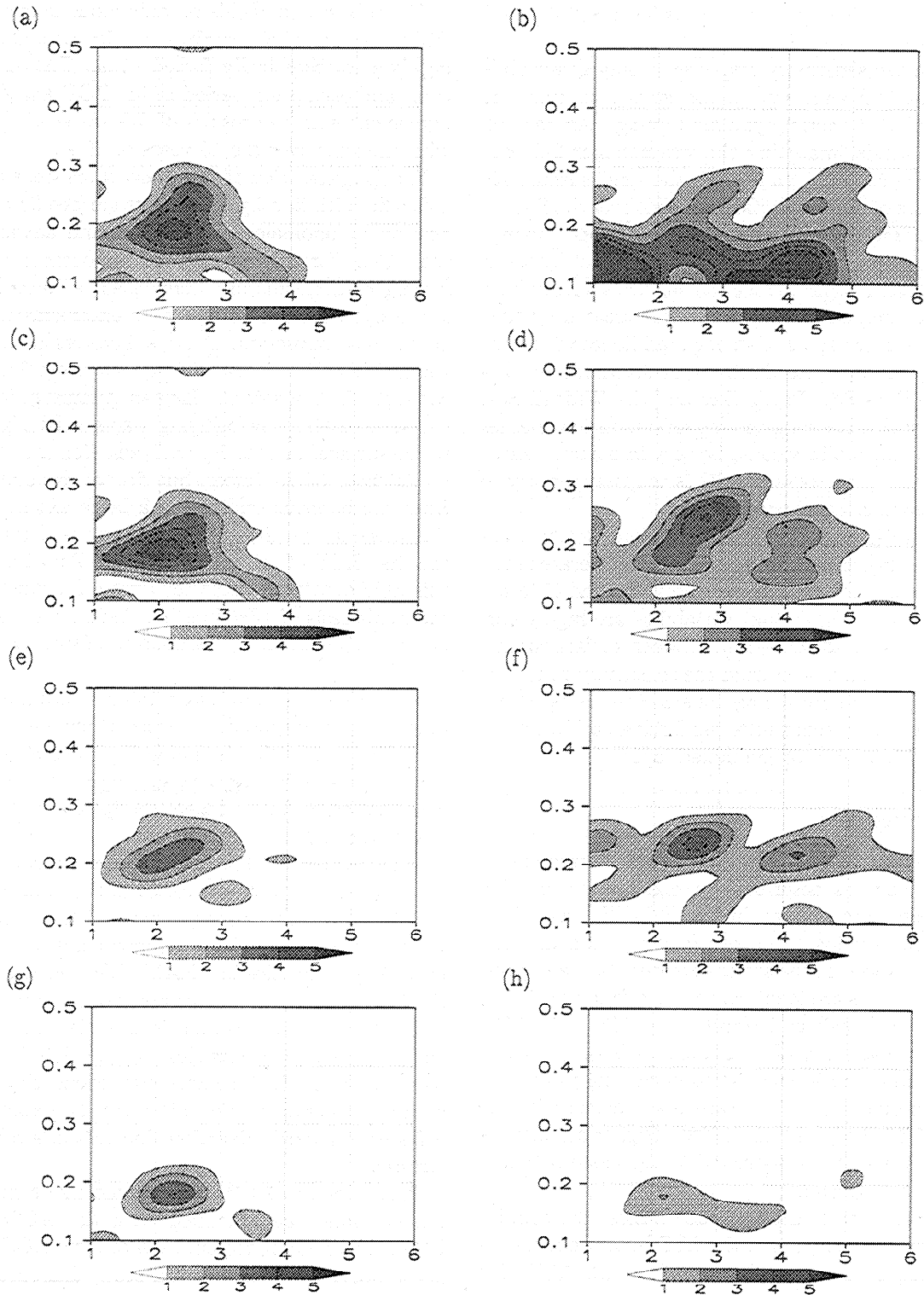
Figure 10. Squared amplitudes (gray scales) of the wavenumber-frequency decomposition of (a) temperature and (b) salinity variability for the basic run, (c) temperature and (d) salinity variability for the run with no freshwater flux H anomalies, (e) temperature and (f) salinity variability for the dynamic forcing run, and (a) temperature and (b) salinity variability for run with thermodynamic forcing. The anomalies are averaged over 46°S-61°S. The squared amplitudes are averaged over the 75, 150, 250 and 450 m layer. The horizontal and vertical axes denote the frequency (cycles per year) and the longitudinal wavenumber, respectively. See Table 2.

convection. In this way, early anomalies in salinity and temperature are created.

Secondly, the sensitivity response to only Q variability (Figures 10g and 10h) is too strong to rule out the possibility of thermodynamic forcing. Anomalous meridional winds (matching the wavenumber 2-3 pattern; see Figure 2a.) can bring the cold surface air temperatures of the Antarctic continent over the Southern Ocean. The associated anomalous surface cooling, which is captured by the Q variability and not by the τ variability, can further reduce the surface stability, and salinity and temperature anomalies are created by convection. The three spots of strong meridional winds are remarkably close to the three major Antarctic embayments, the Ross Sea, Prydz Bay and the Weddell Sea, where, normally, a strong cooling exists. In this mechanism, sea ice variablility could be very important. However, the sea ice response of LSG is too rudimentary to allow any further conclusions.

Finally, we stress that the dynamic and the thermodynamic forcing mechanisms both largely operate in the same wavenumber 2-3 pattern: The $\nabla \times \tau$ and Q (especially the sensible heat flux) variability are highly correlated because of the close link between surface cooling and winds. We have seen from the sensitivity runs that both are capable of producing the ACW patterns. Probably, the two mechanisms are reinforcing each other by reducing the stability of the mixed layer.

7. Conclusions

The major atmospheric features of the Antarctic Circumpolar Wave as described by, e.g., *White and Peterson* [1996], are present in the ECMWF reanalysis (ERA) surface fields. The oscillation period and the propagation speed of the surface temperature and pressure p_0 anomalies are identical to those found by *White and Peterson* [1996] and *Jacobs and Mitchell* [1996]. However, propagation of p_0 anomalies is only present in the period of 1985-1994. Nonpropagating p_0 anomalies in the period of 1979-1985 are in agreement with the findings of *Christoph et al.* [1998]. Higher amplitudes of the ACW mode are restricted to the eastern Indian and the Pacific Ocean.

When forced with ERA surface fluxes, the salinity and temperature outputs of the LSG ocean model contain a mode of interannual variability with ACW-like characteristics: Temperature and salinity anomalies, originating from roughly 70°E and 180°E and reappearing every 4 to 5 years, propagate eastward through the Southern Ocean and decay after having passed through Drake Passage. This signal is also captured in the LSG output of anomalous surface elevation and oceanic convection. The oscillation period and the eastward propagation of the anomalies are sustained to a depth of a few hundred meters. Higher amplitudes and a more pronounced eastward propagation are present in the period of 1985-1994.

The robustness of this oceanic mode is confirmed by POP analyzes of the surface salinity anomalies resulting from stochastically forced runs. The spatial patterns and oscillation period of the POP analyzes are in agreement with the results of *Weisse et al.* [1999] and with the runs over the 15 years of ERA.

For the generation of the mode, three steps are distinguished: Initiation by anomalous surface fluxes, amplification by anomalous convection, and advection with the ACC. For the initiation of the oceanic mode, two forcing mechanisms are formulated, a thermodynamic and a dynamic one. Both the mechanisms trigger the anomalous convection. The first involves anomalous advection of cold air and subsequent anomalous surface cooling. In the second, Ekman pumping destabilizes the stratification by bringing warm subsurface waters to the surface. Sensitivity analyzes with the LSG model are in favor of the latter, but do not exclude the first. Both mechanisms operate to a large extent in a spatial wavenumber 2-3 pattern, which is determined by the first EOF of the p_0 variability. The time series of this EOF depicts no preferred timescale, which confirms the hypothesis of *Weisse et al.* [1999], who explain the oceanic ACW mode by the concept of stochastic climate models.

An amplifying (and maintaining) mechanism for the anomalies is proposed in terms of anomalous convection. This convection is enabled by the marginal stratification present in large areas of the Southern Ocean. It can counteract the turbulent dissipation of the anomalies by the ACC.

Much evidence is found for a passive advection of the ocean anomalies with the ACC. In the hindcast run the speed ratio of the atmospheric and the oceanic eastward moving anomalies is proportional to the ratio of local ACC velocities in FRAM [*Webb et al.*, 1991] and the LSG model. The latter are too low (up to a factor of 2). Furthermore, comparison of the stochastic runs with the *Hellerman and Rosenstein* [1983] based climatology and the ERA climatology reveals that a shorter oscillation period in the latter can be explained from a faster eastward advection due to the stronger wind stresses.

Phases of the ACW-like oceanic mode in the LSG model cannot be identified with the ACW mode in ERA; the model representation of local ACC velocities is too poor. Nevertheless, this study demonstrates that a one-way atmosphere to ocean coupling is sufficient to generate surface temperature anomalies with an ACW-like signature.

References

Arpe, K., L. Bengtsson, and E Roekner, The impact of sea surface temperature anomalies on the variability of the atmospheric circulation in the ECHAM3 model, in Research activities in atmospheric and oceanic modelling, edited by G.Boer,*Rep. 18*, pp. 7.18–7.20, World Meteorol. Organ., Geneva, 1993.

Christoph, M., T.P. Barnett, and E. Roeckner, The Antarctic Circumpolar Wave in a coupled ocean–atmosphere GCM, *J. Clim.*,*11*, 1659–1672, 1998.

Connolley, W.M., Variability in annual mean circulation in southern high latitudes, *Clim. Dyn.*,*13*, 745–756, 1997.

Gibson, R., P. Källberg, and S. Uppala, A. Nomura, A. Hernandez, and E. Serrano., ERA description, *ECMWF Re-analysis Proj. Rep. Ser. 1*, Eur. Cent. for Medium-Range Weather Forecasts, Reading, England, 1996.

Hasselmann, K., Stochastic climate models, 1, Theory, *Tellus*, *28*, 473–485, 1976.

Hellerman, S., and M. Rosenstein, Normal monthly wind stress over the world ocean with error estimates, *J. Phys. Oceanogr.*, *13*, 1093–1104, 1983.

Jacobs, G.A., and J.L. Mitchell, Ocean circulation variations associated with the Antarctic Circumpolar Wave, *Geophys. Res. Lett.*, *23*, 2947–2950, 1996.

Karoly, D.J., Southern hemisphere circulation features associated with El Niño-Southern Oscillation events, *J. Clim.*, *2*, 1239–1252, 1989.

Levitus, S., Climatological atlas of the world ocean, *NOAA Prof. Pap. no. 13*, U.S. Govt. Print. Off., Washington, D.C., 1982.

Maier-Reimer, E., U. Mikolajewicz, and K. Hasselmann, Mean circulation of the Hamburg LSG OGCM and its sensitivity to the thermohaline surface forcing, *J. Phys. Oceanogr.*, *23*, 731–757, 1993.

Qiu, B., and F.-F. Jin, Antarctic circumpolar waves: An indication of ocean–atmosphere coupling in the extratropics, *Geophys. Res. Lett.*, *24*,, 2585–2588, 1997.

Saravanan, R., and J.C. McWilliams, Advective ocean-atmosphere interaction: An analytical stochastic model with implications for decadal variability, *J. Clim.*, *11*, 165–188, 1998.

von Storch, H., and F.W. Zwiers, *Statistical Analysis in Climate Research*, Cambridge University Press, New York, 1997.

Webb, D.J., P.D. Killworth, A.C. Coward, and S.R. Thompson, *The FRAM Atlas of the Southern Ocean*, Nat. Environ. Res. Counc., Swindon, England, 1991.

Weisse, R., U. Mikolajewicz, A. Sterl, and S.S. Drijhout., Stochastically forced variability in the Antarctic Circumpolar Current, *J. Geophys. Res.*, , in press, 1999.

White, W.B., and R.G. Peterson, An Antarctic Circumpolar Wave in surface pressure,wind, temperature and sea-ice extent, *Nature*,*380*, 699–702, 1996.

Woodruff, S.D., R.J. Slutz, R.L. Jenne, and P.M. Steurer, A comprehensive ocean–atmosphere data set, *Bull. Am. Meteorol. Soc.*, *68*, 1239–1250, 1987.

H. Bonekamp, H., A. Sterl, and G.J. Komen, Royal Netherlands Meteorological Institute, P.o. Box 201, 3730 AE De Bilt, Netherlands. (bonekamp@knmi.nl)